Available online at www.sciencedirect.com
ScienceDirect
International Journal of Solids and Structures 45 (2008) 2881–2896
INTERNATIONAL JOURNAL OF SOLIDS AND STRUCTURES
www.elsevier.com/locate/ijsolstr

Relating cellular structure of open solid food foams to their Young's modulus: Finite element calculation

S. Guessasma [a,*], P. Babin [a], G. Della Valle [a], R. Dendievel [b]

[a] INRA – BIA, Rue de la géraudière, Nantes 44316, France
[b] GPM2 – ENSPG, BP 46, 38402 Saint Martin d'Heres, France

Received 12 May 2007; received in revised form 29 November 2007
Available online 15 January 2008

Abstract

This paper investigates the role of structure on Young's modulus of open cell materials of relative densities between 0.1 and 0.3. The cellular solid is obtained by generating mixture size of spherical voids using the Random Sequential Addition – RSA algorithm. The relative density of the material is controlled by increasing void number and overlap. Structural effects consider mainly a Gaussian distribution of spherical void size of varying width, distribution centre and void overlap distance. Finite element method is used to calculate effective Young's modulus using a regular meshing scheme of 3D typical cellular solids and Conjugate Gradient solver. It is found that sphere overlap has the largest effect compared to sphere distribution width for a given density. A large scatter in the wall thickness distribution is predicted when overlapping is increased or when the width of sphere size distribution is decreased. Increased rigidity is found to be correlated to particular arrangement of mixture size spheres which is pointed out using the Pair Correlation Function. Experimental evidence of the role of void overlapping is treated in the case of bread crumbs structures determined using X-ray tomography. The scatter of effective Young's modulus for a given relative density is sensitive to void overlapping.

Keywords: Young's modulus; Finite element method; Random sequential addition; Low relative density material; Overlapping

1. Introduction

Cellular solids and particularly foams are used in many applications where thermal insulation, light weight structures, filtering, flotation are needed. A basic understanding of the mechanical properties of cellular solids is a prerequisite to allow product design with improved end-uses properties.

Linear elasticity of open-cell and close-cell foams was already described (Gibson and Ashby, 1997; Evans et al., 1998; Roberts and Garboczi, 2001; Roberts and Garboczi, 2002). Power laws relating the mechanical properties to the relative density were suggested, either numerically, or experimentally. But they concern generally ordered materials and arrangements with small cell wall irregularities (Chen et al., 1999) or with struc-

* Corresponding author. Tel.: +33 (0) 2 40 67 50 36; fax: +33 (0) 2 40 67 51 67.
E-mail address: sofiane.guessasma@nantes.inra.fr (S. Guessasma).

0020-7683/$ - see front matter © 2008 Elsevier Ltd. All rights reserved.
doi:10.1016/j.ijsolstr.2008.01.007

tural imperfections (Grenestedt, 1998). Attempts to consider the random structure of open-cell structures were undertaken (Poutet et al., 1996; Roberts and Garboczi, 2002). However, few of them considered the characterisation of the complex network of the void structures in terms of structural attributes. In this paper, the random void media is represented by random arrangement of spherical voids. The idea is to control both cell size distribution and void connectivity parameters of the open cellular solid, in addition to relative density. Then, these structural attributes are related to the effective Young's modulus in order to suggest improvement of the scaling law relating the mechanical properties to the relative density of the cellular solid.

This approach is all the more important in the field of biopolymer based solid foams for which the experimental generation of cellular structures with controlled characteristics is still a challenge (Kanit et al., 2006). Furthermore, their mechanical properties, specially for food products (bread, biscuits, etc.) which have generally a very low relative density (<0.3), control the texture and, finally, consumer's acceptance.

2. Mathematical model

2.1. Void structure generation

In many situations, cellular solids exhibit major structural changes during material processing. One of the major processes is foaming by bubble nucleation, growth and coalescence upon supersaturated solution of gas dissolved in a matrix (Amon and Denson, 1984). Random packing of spherical voids is then a realistic model to generate such foam structure. In this study, the RSA is used as it represents a good approximation of bubble arrangements induced by such processes, as illustrated by the comparison between cellular structures generated using this technique and the image of a bread crumb determined using X-ray tomography (Fig. 1). A review of the Random Sequential Addition (RSA) algorithm can be found in works by Evans (1993), Talbot et al. (1991), for instance.

Random packing of non-overlapping spheres has been shown to lead to relative density of the solid foam larger than 0.4 (Lavalle et al., 1999; Williams and Philipse, 2003; Donev et al., 2004; Gan et al., 2004). The largest fraction of sphere arrangement related to random close packing (RCP) is 0.64 for spheres of equal size (Williams and Philipse, 2003; Donev et al., 2004), whereas with ordered packing like fcc or hcp lattices, it reaches about 0.74. Then, material relative density is larger than 0.26, which is still large regarding the field of applications of solid foams.

Nevertheless, such a technique leads to low sphere fractions (less than 0.64) and, in some conditions, requires large sample size in order to guarantee the isotropy of the structures (Clarke and Wiley, 1987). Thus, the use of the RSA to generate open cell structures requires a specific handling of the cells size if low relative density (<0.3) is aimed.

The technique is improved to randomly generate spherical voids of different sizes, according to a Gaussian distribution of voids with controlled centre position r_0 and width σ/r_0, expressed with respect to r_0 (Fig. 1a). Periodic boundary conditions are used so that any sphere in contact with any face of the volume is replicated in the opposite face. The use of such type of boundary conditions allows to minimize the required sample size.

In order to lower the density of the material, void spheres of various sizes are mixed and allowed to overlap at a controlled distance using the RSA technique. This is obtained with an inter-sphere spacing lower than the sum of sphere radii. Thus, we define an overlap distance δ by the distance from centre to centre C_{ij} separating the centres of adjacent sphere i and j minus the sum of sphere radii r_i and r_j:

$$\delta = C_{ij} - (r_i + r_j) \tag{1}$$

δ takes negative values when spheres overlap, which is always the case if relative density is lower than 0.36 (i.e., void fraction larger than 0.64 in the case of monomodal void sphere distribution). In the following, we refer to large overlap when δ is negative and has a large absolute value.

The packing starts by selecting a random position of the first sphere. Further sphere addition is allowed if the distance between any of the existing spheres and the new one is larger than the overlap distance. In our RSA algorithm, if an addition of a sphere is not possible over 10^5 trials, the whole sphere configuration is rejected. This event occurs especially in the case of a large number of spheres and lowest relative densities,

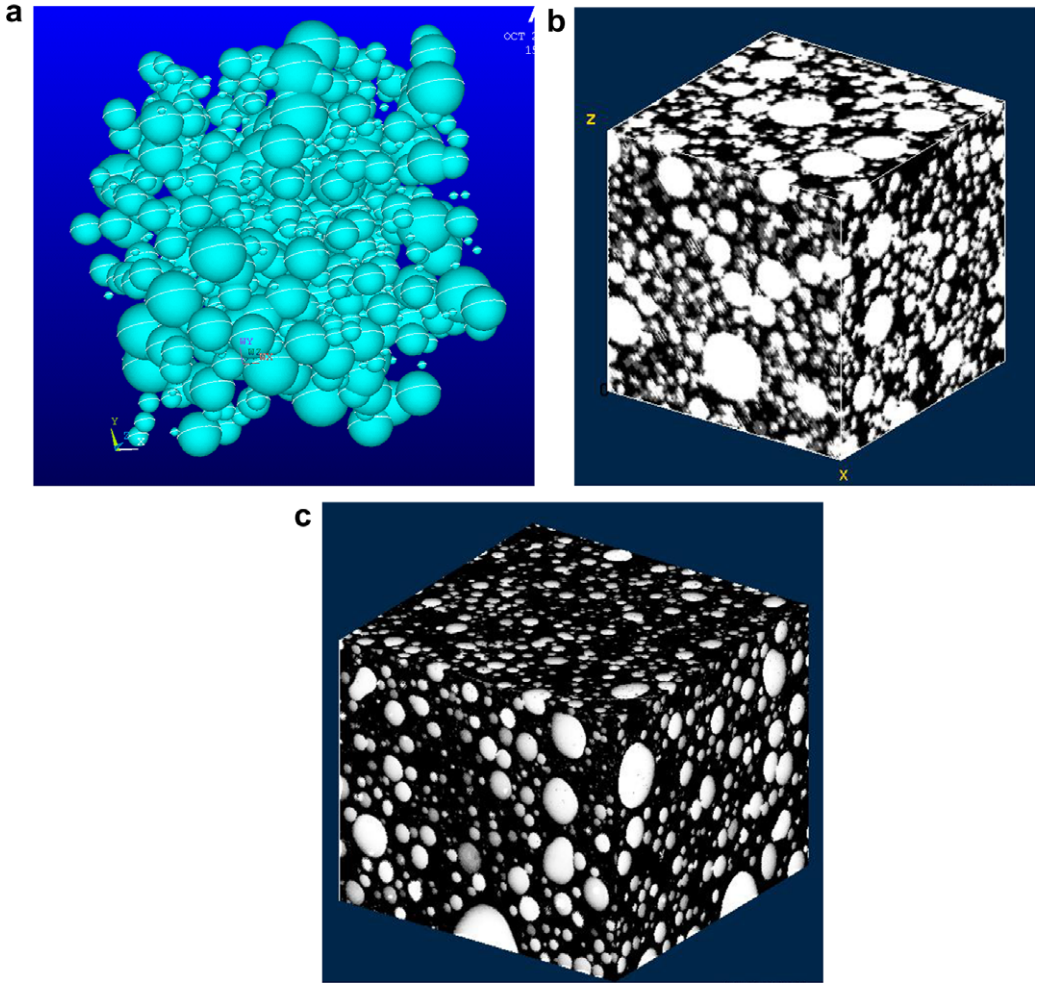

Fig. 1. Cellular structure generated using random sequential addition (RSA) algorithm showing (a) spherical packing, (b) virtual 3D structure and (c) a 3D image of a bread dough determined using X-ray tomography (relative density = 0.4, volume = 0.7 cm^3) (ESRF-Grenoble, France).

because few sphere configurations are available. Large overlaps values allow to vary the relative density over a large range.

The generated solid foam is represented by a 3D image discretized by a cubic grid which contains a maximum number of voxels V. The void structure is created by counting up the voxel units in the spheres knowing their positions and radius, so that each remaining voxel corresponds to a solid element (Roberts and Garboczi, 2001, 2002). The amount of solid elements defines the relative density (ρ), which is calculated as the sum of solid units in the cellular structure:

$$\rho = \sum i/V \tag{2}$$

where i is a solid phase element. V is the total volume of the solid expressed in voxels.

Overlap distance and size distribution are both parameters of the relative density. But they also modify the number of void spheres required to obtain the cellular structure, as illustrated in Fig. 2. Relative density values lower than 0.3 cannot be obtained for $|\delta| < 3$ voxels in these conditions. Each sphere configuration is validated if the number of trials necessary to find a position for any sphere in the structure does not reach 10^5. Then, five structures are generated for each configuration to obtain the variability of the overall density at a fixed value of the number of sphere voids. Changing the number of spheres would modify slightly the

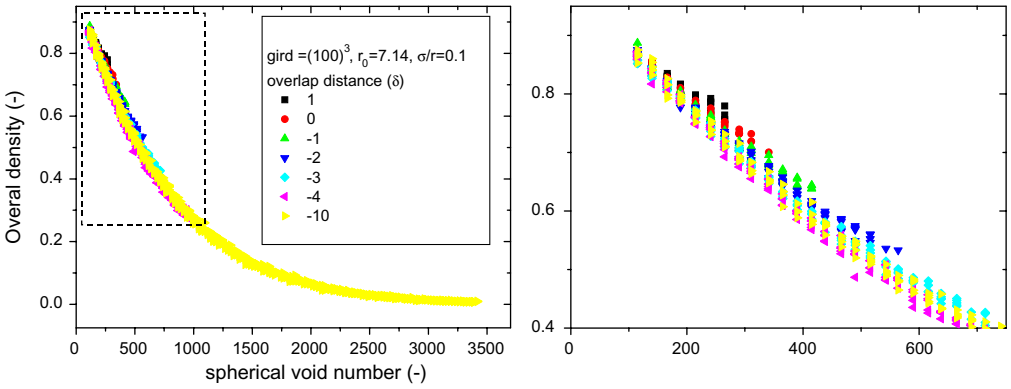

Fig. 2. Overall density of the material as function of void number for different overlap distances. Units are given in voxels.

effective properties. At this stage, the variability of sphere number is not described in the ensuing discussion and all it stands for.

The variability of relative density depends on δ value and represents 1% for small overlaps ($|\delta| > 3$) and 6% for large overlaps ($|\delta| > 5$). Overall, the smallest possible ρ value is also sensitive to void size distribution parameters (r_0, σ/r_0). In the case of large r_0 and small σ/r_0 values, lowest ρ values are obtained with large overlap distances δ.

When $|\delta|$ values are small, typically less than 2% with respect to the sample size, low values of relative density are obtained only when a transition occurred from fully random to slightly ordered packing. The long-range ordering appears mostly as a finite-size effect which can be avoided by using large sample sizes (Sherwood, 1997).

The time spent to generate spheres is also a matter of concern as RSA technique is known to be time consuming. For example, when applying the conditions (relative density $\rho = 0.2$, distribution centre $r_0 = 7.14$, distribution width $\sigma/r = 0.1$), only 20 trials per sphere position are needed to obtain the void structure for $\delta = -10$, whereas this number increases to 10^2 for $\delta = -7$ and to 10^4 for $\delta = -5$. So, obtaining ordered structures with small overlaps is meaningful because a reasonable simulation time of sphere packing is obtained only with small box sizes, which favours ordered structures (Sherwood, 1997).

Fig. 3a shows the number of void spheres for a typical volume $V = 100^3$ and three different values of relative density. The number of spheres is less than 300 for the distribution centre $r_0 = 14.29$, which means that, in such distributions, large spheres are not well represented, statistically. Meanwhile, with $r_0 = 7.14$, large numbers of large spheres are available but smaller ones are less spherical, because of voxel size. The radii gap noticed between $r = 9$ and $r = 11$ is due to the truncation performed to preserve void size distribution symmetry. Indeed, the simulated distributions are characterized by tail truncation because large spheres add large volume fraction, as shown by the sphere volume distribution represented for various relative density values in Fig. 3b. Selecting large radii classes are no more possible when the associated sphere number is lower than unity, so, truncation is also imposed to small size classes in order to guarantee the distribution symmetry. Increasing the distribution width increases the number of spheres per unit volume, for a given relative density (Fig. 3c).

2.2. Wall thickness distribution

The main characteristics of the open cell structures are calculated for different sphere distribution widths and overlap distances. The first structural attribute calculated is the wall thickness. Cell wall size distribution is obtained using 3D granulometry analysis. An iterative process is applied on binarised structures using successive erosion and dilation operators with an octahedral structuring element which size is associated to wall thickness class (Russ, 1990; Jahne, 1997). Histograms are obtained representing the volumic fraction of solid phase are obtained as function of wall thickness value.

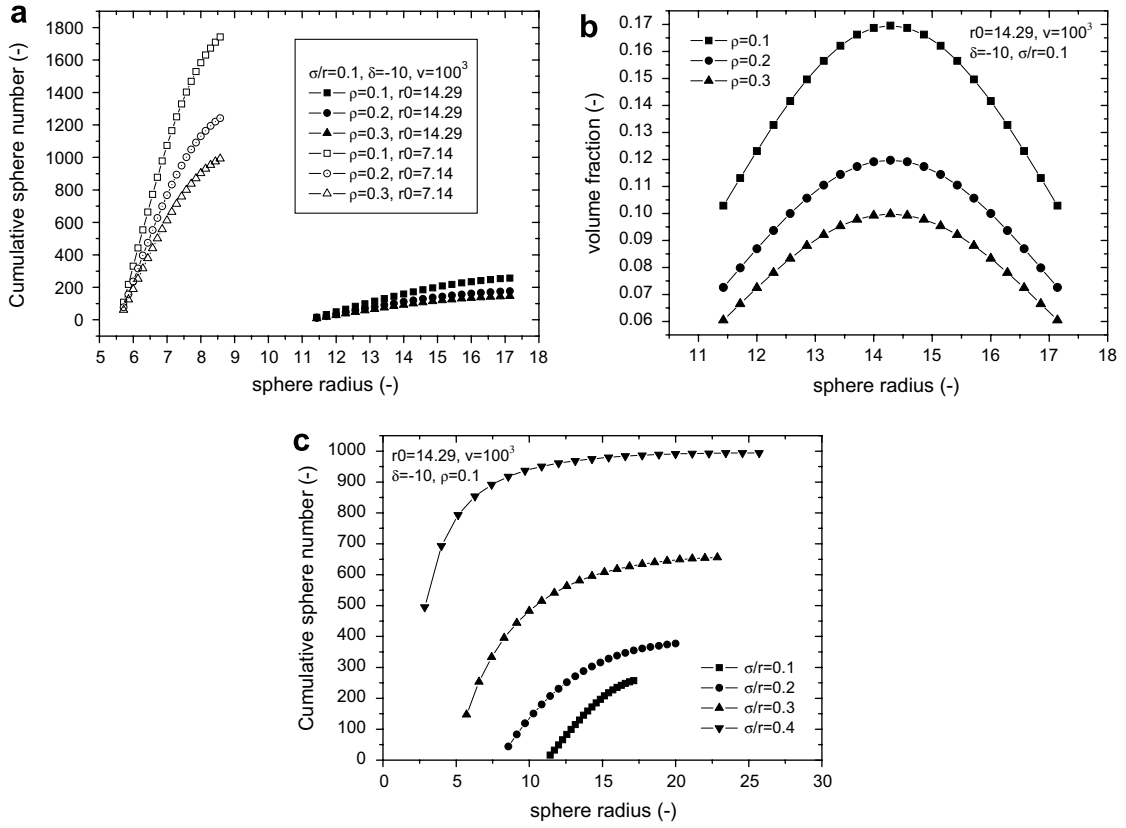

Fig. 3. (a) Cumulative number of spherical voids as function of sphere radius for two size distribution centres showing the spherical void number used to generate cellular solids. (b) Volume distribution as function of relative density. (c) Cumulative number of spherical void as function of sphere radius for various distribution widths.

Fig. 4 shows wall thickness distributions for various values of relative density, sphere distribution width and overlap distance. Broader distributions are associated to large ρ values. Assuming the condition ($\delta = -20$, $r_0 = 14.29$, $\sigma/r = 0.1$), average wall thickness increases from 12 to 22 units for ρ increasing from 0.10 to 0.38. Despite the wall thickness increase, the cellular structures still remains open.

A less significant influence is found for sphere width distribution on wall thickness distribution (Fig. 4b). When σ/r decreases from 0.4 to 0.1, average wall thickness is found to increase from 8.2 to 10.5. Size distributions exhibit large end tails including classes of larger size, suggesting that large scatter of wall thickness values is correlated to lower σ/r values and that "sphere packing" is improved when radii are more dispersed. Here, packing is related to the lowest distance which allows spheres to be close to each other. This argument has a special meaning which is treated in details when calculating the Pair Correlation Functions (PCF) of the open structures.

Fig. 4c shows the effect of overlap distance on wall thickness. An increase of $|\delta|$ is found to shift the whole distribution towards large thickness classes, and average thickness varies from 7.5 to 12.25 when $|\delta|$ increases from 10 to 20), which suggests an increase of the disorder of cellular structures, as further assessed by the PCF. Overall, δ has more significant effect on cellular structure, than ρ and σ/r parameters.

2.3. Pair correlation function

In order to describe the characteristics of sphere overlapping, the pair correlation function $g(r)$ is used as a second structural attribute (Stillinger and Torquato, 2004). This function is related to the probability of finding the centre of a given sphere at a given distance from the centre of another sphere.

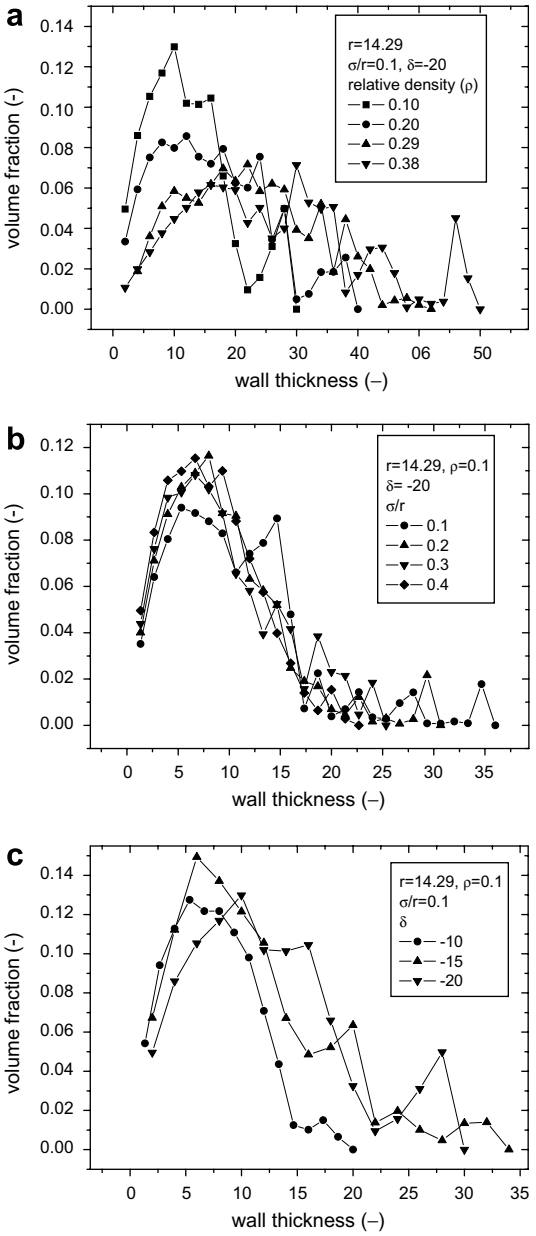

Fig. 4. Wall thickness distribution as function of (a) relative density, (b) width of sphere size distribution and (c) overlap distance (wall thickness class is in voxel units).

$$g(r) = \frac{\left(\sum_i \sum_{j \neq i} \Delta\langle r - C_{ij}\rangle\right)}{\frac{4\pi r^2 \mathrm{d}r}{\frac{N_{\mathrm{tot}}}{V}}} \tag{3}$$

where N_{tot} is the total number of spheres in the volume V. C_{ij} has the same meaning as in (Eq. (1)).

This function is roughly characterized by nearest neighbour peaks, followed by possible secondary peaks, if the cellular structure has any cell order. In particular, random or glass like structures are characterized by a short distance peak and vanishing fluctuations towards $g(r) = 1$ when r increases. Multiple peak profile indicates that the structure displays a long range order, like crystallinity for instance. Thus, $g(r)$ is used here to assess the randomness of cell distribution or the tendency to organised packing.

In fact, analytical expressions for $g(r)$ are available for several random media models such as Boolean models (Mattfeldt and Stoyan, 2000; Monetto and Drugan, 2004). However, $g(r)$ evaluation assumes that we are able to compute the two-point phase probability function (Quintanilla, 2006). This is a quite difficult task, if we consider that RSA is a selective process, for which the phase probability function depends on generation time. Even if this problem is solved, analytical expressions are normally not available in the case where void polydispersity is implemented (Quintanilla, 2006).

Fig. 5 shows two examples of PCF for different values of σ/r and δ parameters. Here, we use the correction $g(r) - 1$ instead of $g(r)$. A zero value tail is found common to all sketches indicating the absence of sphere centres at short distances ($r < 5$ voxels). This limiting distance depends on δ, r_0 and σ/r. Indeed, the tail is wide when $|\delta|$ is small (Fig. 5a) or when σ/r is large (Fig. 5b). Both results indicate a repulsive character of the sphere overlapping following (Eq. (1)), either for larger void size distribution or for decreasing the absolute value of overlap distance. The presence of a large first peak in the case of $\delta = -20$ demonstrates the large disordered cellular structure pointed out by the predicted large variability in wall thickness distribution (Fig. 4c).

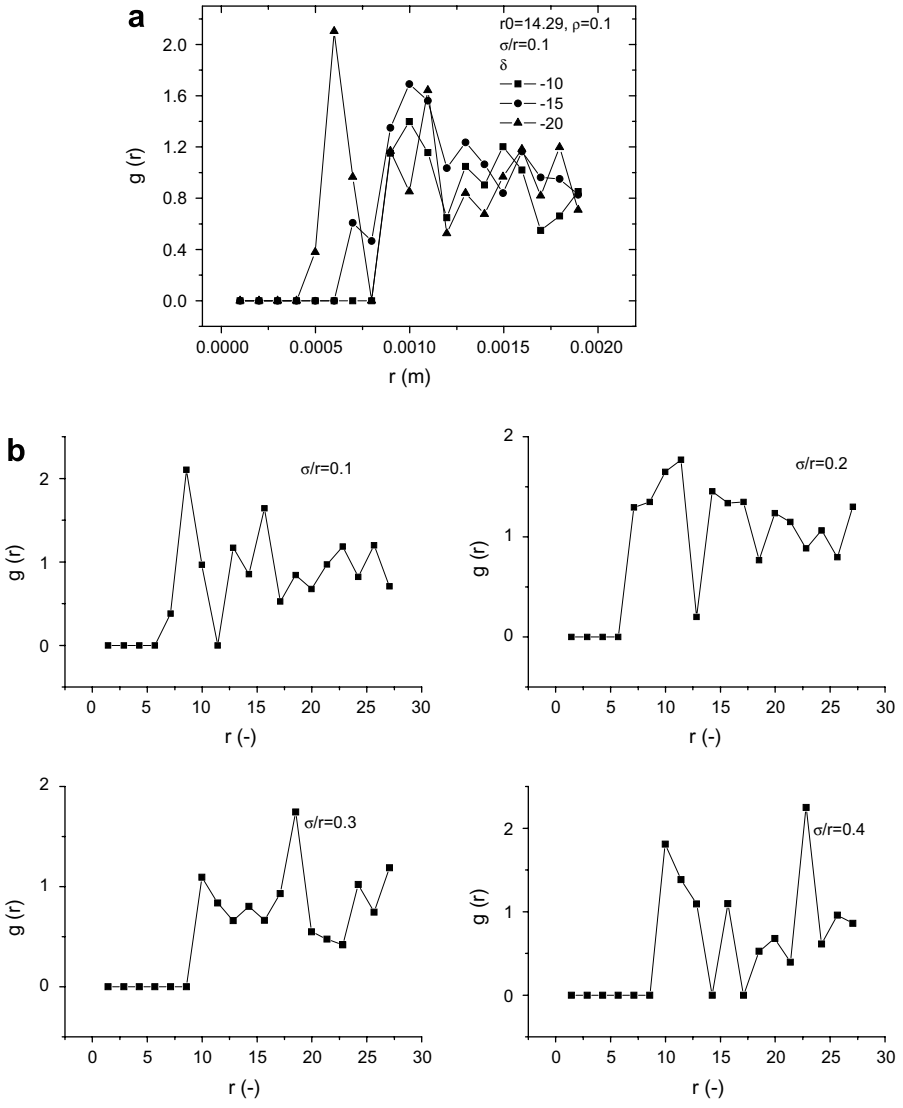

Fig. 5. Pair correlation function versus (a) overlap distance and (b) sphere size dispersion for $\delta = -20$, $r_0 = 14.29$.

Randomness decreases when the ratio σ/r increases (Fig. 5b), indicating that large spheres tends to be surrounded by small spheres and reciprocally. Thus, a tendency to organized overlapping occurs with large σ/r values.

3. Finite element calculation

3.1. Meshing, boundary conditions and computation time

Finite element method (FEM) is used to estimate the relative Young's modulus E of the cellular structures. The ANSYS[1] code is used to solve the linear elastic problem for homogeneous isotropic conditions of the solid phase. The elastic energy is minimised, through an iterative process, using a preconditioned conjugate gradient solver (PCG). The density of the solid phase is given an arbitrary value, and only relative density ρ is modified. Young's modulus of the solid material is attributed an arbitrary value and the result of computations is a relative Young's modulus value. The periodic boundary conditions are used with a combination of a finite displacement applied on given face nodes, and fully constrained nodes against displacement on the opposite face through the same axis. These conditions correspond to a uniaxial compression test. For example, loading in X direction assumes that $UX = 0$ for $X = 0$ and $UX = \mathrm{U}$ for $X = L$ where L is the edge length. Constraint equations are $UYi + UYj = 0$ and $UZi + UZj = 0$ for homologue nodes i,j belonging to lateral faces.

The solid phase of the open cell structures is meshed using the structured mesh generation technique (Topping et al., 2000; Maire et al., 2003) assuming that each voxel is a 8-node cubic element (Solid45 under ANSYS). Such meshing does not provide the best quality meshing compared to irregular schemes but it avoids significant meshing errors in the case of impenetrable particles models. It is assumed that the material elasticity model is isotropic.

The discretisation level of the system corresponds to the maximum number of elements per edge for a fixed volume $V = L^3$. It corresponds to the spatial resolution used for the microscopic analysis, like X-ray microtomography for instance (Kanit et al., 2003).

For $\rho < 0.2$, a typical grid $V = 150^3$ on a 3 GHz computer with 1 Gbytes of RAM gives a calculation time of 210 min. A smaller grid (100^3) allows a relative error, with respect to the modulus (Fig. 6a), lower than 10% for $\rho \geqslant 0.2$ with typical runs taking less than 60 min.

Fig. 6b–d illustrate typical structures under different discretisation levels for a given density and void sphere distribution ($\rho = 0.1, \sigma/r = 0.1,$). In the case of Fig. 6b, some discontinuities in the solid phase appear and this may affect significantly the finite element calculation. Even for the largest discretisation levels (Fig. 6c and d), some discontinuities still remain which are correlated to the amount of missing walls in the structure. One way to avoid discontinuity effects is to keep only the largest connected solid object. However, with this method, large variations of relative density are expected, especially with large overlap distances. The other way, as much arbitrary, is to introduce link units which do not induce large variation of relative density and keep the main characteristics of the cellular solid. In the following, this methodology is experienced.

3.2. Meshing resolution and determination of REV in FE calculation

The resolution and the REV are determined according to the relative variations of relative density and modulus. The scatter in ρ and E is calculated based on the variation of the effective properties as function of the discretisation level L:

$$\%\, ij = \mathrm{AVE}\left(\frac{\mathrm{STD}(i,L)}{\mathrm{AVE}(i,L)}, j\right) \tag{4}$$

where AVE and STD refer to the average value and standard deviation operator on variable i with respect to L. j represents one of the studied parameters (σ/r, δ, r_0). i represents either ρ or E, with E being the average of

[1] ANSYS, Inc. Southpoint 275 Technology Drive, Canonsburg, PA 15317.

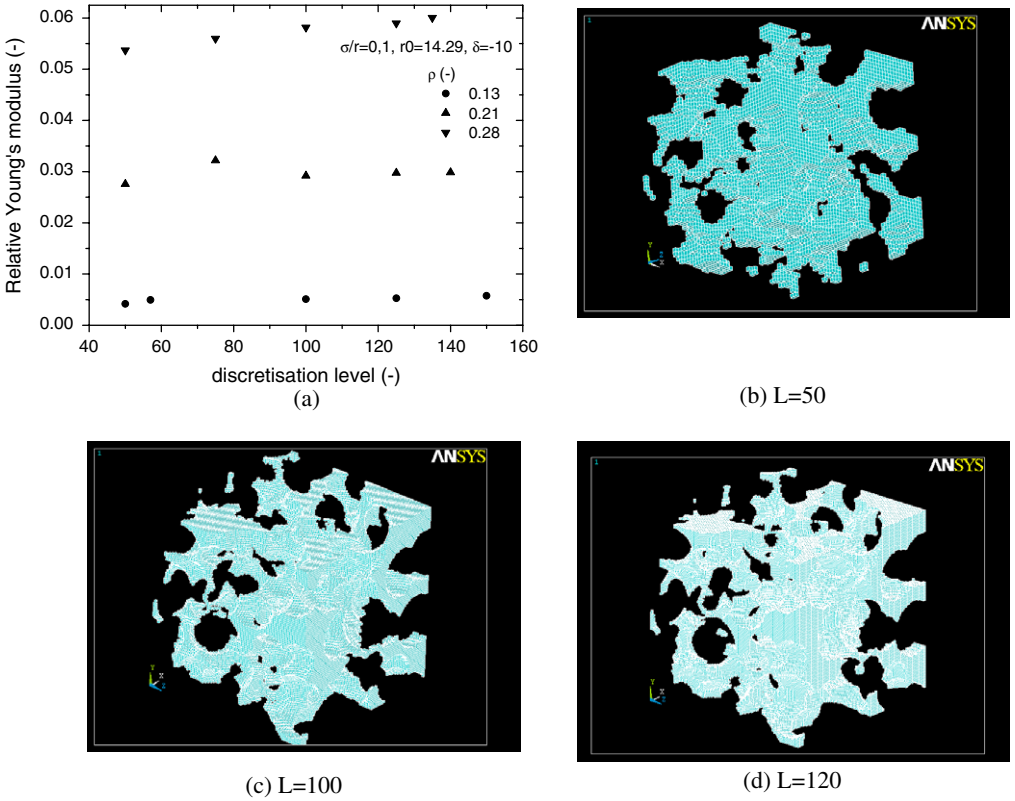

Fig. 6. (a) Effect of discretisation level on relative Young's modulus prediction for three relative densities. Note that element size is L/discretisation level, where L is the edge length of the cellular solid. (b–d) Typical cellular structures generated with different discretisation levels (the maximum voxel number per edge is L).

the moduli values calculated in the three main directions x, y and z. The variability of E in space direction is calculated by:

$$\mathrm{MAX}[(\%E_xj, \%E_yj, \%E_zj) - \%Ej] \tag{5}$$

where MAX is the maximum operator.

The lower is the discretisation level, i.e. the coarser the mesh, the higher is Young's modulus variability. Results in Table 1 show that the variability of E, with respect to the generation parameters (ρ, $\sigma/r, \delta, r0$), is larger (between 8% and 16%) than that of ρ and than the contribution due to space directions. Overall, the sensitivity to space directions X, Y and Z represents less than 3%. The small variability of ρ (<0.5%) is attributed to the link units which increases the connectivity of the solid phase. Finally, r_0 has the largest effect on the variability of E and ρ, in the range tested.

Sampling is performed on meshed structures, for same discretisation L, by selecting a small cubic region representing a volume fraction (sampling ratio) from the whole structure (Fig. 7). This volume fraction is representative of the sample (REV) when the variable computed is constant with the sampling ratio, defined by:

Table 1
Variability of relative density and Young's modulus as function of discretisation level and generation parameters

Parameter[a]	Variability of E in X, Y, Z	Variability of E as function of L ($L > 50$)	Variability of ρ as function of L ($L > 50$)
ρ	—	8	0.06
σ/r	1.55	11	0.40
δ	1.54	14	0.32
r_0	2.33	16	0.39

[a] Range of parameters: ρ (0.1, 0.3), σ/r (0.1, 0.4), δ (−5, −12) voxels, r_0 (4,14) voxels.

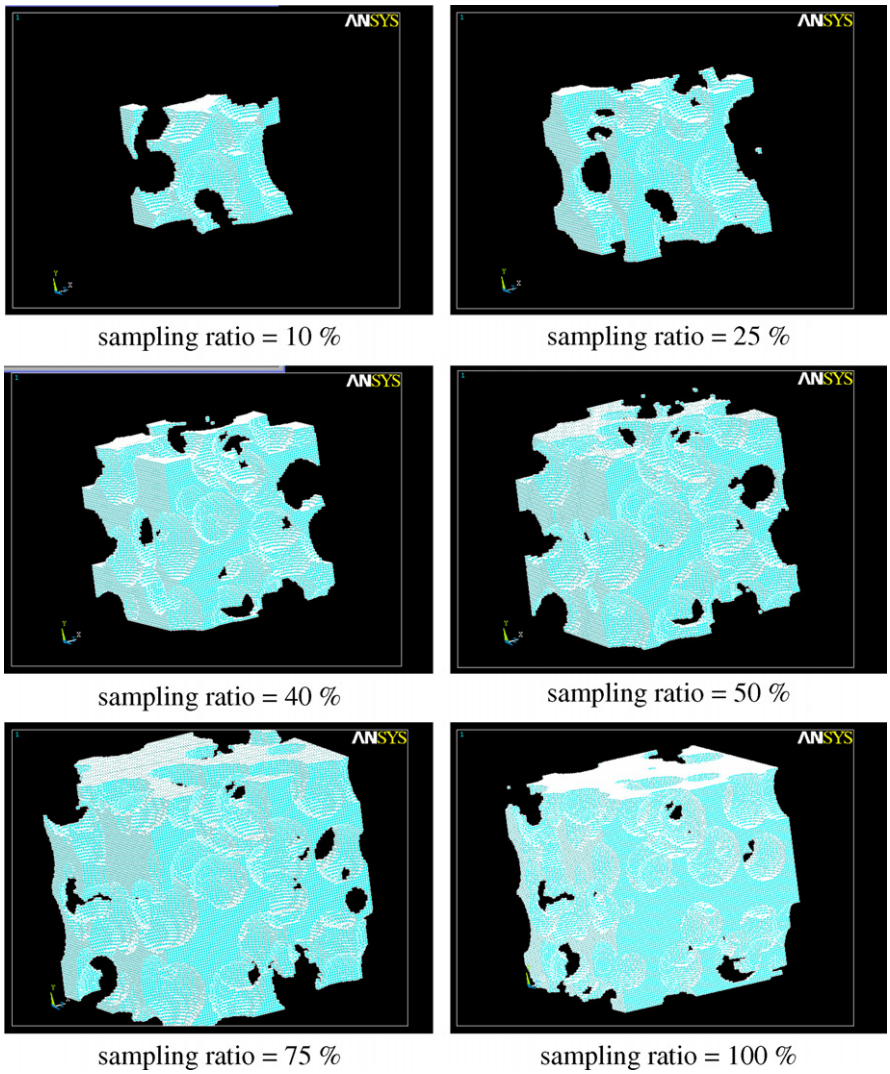

Fig. 7. Typical meshed structures showing sample size effect in open cellular solids ($\sigma/r = 0.1$, $\rho = 0.3$).

$$V = (L * S/100)^3 \tag{6}$$

where S is the sampling ratio.

The predicted variation ratios are calculated in a similar way to that related to discretisation levels (Table 2).

The variability of relative density and modulus in space directions is larger than that predicted for the discretisation level (Tables 1 and 2). The variability of ρ with respect to generation parameters represents up to 5% and is attributed to the fact that sampling adds discontinuities at the frontiers of the cellular structure.

Table 2
Variability of Young's modulus as function of sampling ratio and generation variables

Parameter[a]	Variability of E in X, Y, Z	Variability of E as function of S ($S > 50$)	Variability of ρ as function of S ($S > 50$)
ρ	—	16	2.11
σ/r	1.99	12	4.50
δ	5.00	11	3.27
r_0	8.91	25	4.87

[a] Range of parameters: ρ (0.1–0.3), σ/r (0.1–0.4), δ (−6, −9) voxels, r_0 (4, 14) voxels.

The effect of sampling is significant in the case of ρ with typical variation of the elasticity modulus and relative density of about 40% and 13% for sampling ratios larger than 10%. These variations decrease to about 16% and 2%, respectively, for S values >50. Like for discretisation, r_0 is found to be the most influent on variability of ρ and E. This is due to sampling, which can be expressed as the effect of the ratio of the cell size to the sample size. The relative density is not significantly affected by S and L because of the unit links introduced in the structure. These links improve the connectivity in the cellular structure. In the following, no sampling is performed because of the large variations of E when $S < 100\%$. Moreover, this choice guarantees the conservation of the geometric boundary conditions used in the generation. The resolution of the system is taken as $L = 100$, which represents a good compromise to avoid large variations of E and a suitable calculation time.

4. Results and discussion

4.1. Influence of structure parameters

Fig. 8 shows the decrease of the Young's modulus as function of the value of the centre of the spheres distribution r_0. For a given volume of the material, the decrease of r_0 permits to increase the number of cells and thus to decrease the sample size with respect to cell size. Such correlation is then related to scaling effect in the cellular solid. Brezny and Green (1990a) studied the effect of cell size on the effective Young's modulus and predicted a variability of the modulus with no clear correlation. This variability was attributed to the variability of the solid phase Young's modulus rather than to scaling effects. Other structural considerations explaining the cell size effect were reported (Brezny and Green, 1990b). In open cell alumina, Hagiwara and Green (1987) related the size effect to the increase of the ratio of close cells when the cell size decreases. Dam et al. (1990) attributed the correlation to the decrease of the solid phase Young's modulus, due to the presence of microcracks which appear mostly in the struts surrounding small cells.

Scaling effects can be also predicted by the Cosserat elasticity described by six variables in contrast to the classic elastic solid in which there are only two independent variables (Lakes, 1995). Cosserat effects can be responsible for the increase of the Young's modulus with the decrease of the sample size with respect of cell size (Lakes, 1995; Onck et al., 2001). More recently, Onck et al. (2001) studied the scaling effect in a 2D regular honeycomb. The idea was to attribute the scaling effect to the small contribution of the outer surfaces of the cellular solid which contain walls less constrained. In our case, the slight increase of the effective Young's modulus for smaller cell size can be attributed to the fact that the cellular solid "remembers" less surface effects when the cell size is small (i.e., large number of cells). The contribution of the core region where stiffness is not affected by the end effects becomes then predominant. Our result is qualitatively in good agreement with the result of Onck et al. (2001). A large decrease of the relative modulus is expected when dealing with large spheres ($r0 \gg 10$), because the sample is no more a REV. In the present case (Fig. 8) Young's modulus variation is small because of using periodic boundary conditions.

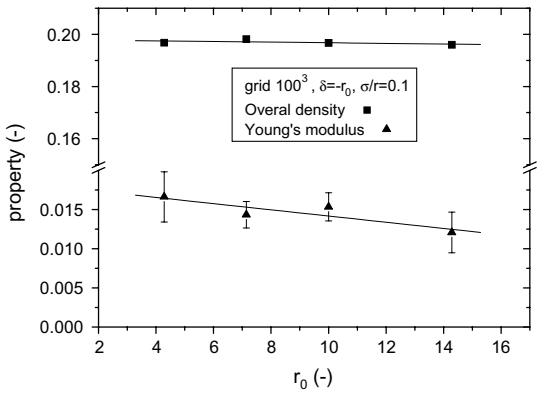

Fig. 8. Sensitivity of Young's modulus and overall density to the centre value of size distribution (r_0).

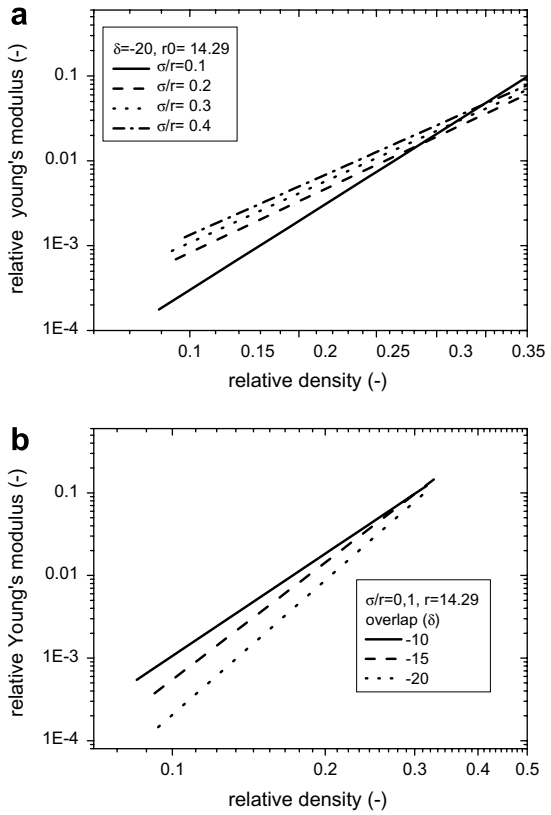

Fig. 9. Relative Young's modulus values as function of relative density. (a) Effect of size distribution width. (b) Effect of overlap distance. Lines are drawn for the best fit and standard deviations are reported in Table 3.

Fig. 9 shows the overall Young's modulus results as function of relative density for different sphere distribution widths and overlap distances.

It is found particularly that an increased stiffness is correlated to cellular structures with large sphere dispersion (Fig. 9a), typically by a factor of 2, when dispersion is increased by 4, for a relative density of 0.15. Because wall thickness profiles indicate that the wall thickness distribution is larger for a decreasing σ/r value (Fig. 4b), the low stiffness is due to a combination of bending and uniaxial deformation mechanisms. The work of Grenestedt and Bassinet (2000) gives a qualitative interpretation of cell wall thickness distribution in the case of close cell solids. They predicted a slight decrease (20%) of stiffness parameters with the increase of the wall thickness dispersion. Another possible interpretation to this result would be related to other geometric considerations as suggested in Fig. 5b. Indeed, organized overlapping can be obtained with large distributions of sphere radii. This result was already reported by Clarke and Wiley (1987) for hard spheres, where packing is found to be improved when increasing the difference between sphere radii. Such organized sphere arrangement is suggested to confer better rigidity to the cellular solid, which can also be explained by a narrower distribution of cell wall size (Fig. 4b).

In the range tested, overlap distance has the largest discriminating effect on the dependence of Young's modulus upon density. The largest modulus values are obtained for the smallest $|\delta|$ value whatever the relative density is (Fig. 9b), and typically increase by a factor of 3, when overlap is increased by 2, for a relative density of 0.15. Again, this result can be interpreted by the decrease of wall thickness dispersion as indicated in Fig. 4c.

Quantitative interpretation of the former results can be given by considering the equation of Gibson and Ashby (1997) which relates Young's modulus to relative density for open cell structures:

$$E = c\rho^n \tag{7}$$

Table 3
Dependence of generation parameters to the exponent and prefactor of the power law relating Young's modulus to relative density

δ (−)	−20				−15	−10
σ/r	0.1	0.2	0.3	0.4	0.2	0.2
Exponent n	3.97 ± 0.47	3.44 ± 0.25	3.31 ± 0.17	3.25 ± 0.39	3.15 ± 0.52	2.96 ± 0.22
Constant C						
MIN	1.55	1.24	1.27	1.14	1.10	1.18
MAX	3.08	1.63	1.58	1.85	2.29	1.58
AVE	2.18	1.42	1.42	1.45	1.58	1.37
Correlation coefficient R^2	0.89	0.99	0.99	0.96	0.97	0.99
Standard deviation SD (%)	34	15	12	25	10	6

where C is a prefactor close to unity and n is an exponent which varies between 1 and 4, depending on whether cells are open or close (Roberts and Garboczi, 2001). The graphs presented in Fig. 9 well show that our results are in line with this theory as confirmed by the correlation factors shown in Table 3.

Coefficients n and C are sensitive to the cellular structure : sphere arrangement and size distribution (Roberts and Garboczi, 2001, 2002). Based on a dimensional analysis of an assembly of beams under flexure, simple models assume that $n = 2$ for open solids with arrangement of isotropic cells (Gibson and Ashby, 1997). Roberts and Garboczi (2002) found that $1.3 < n < 3$, suggesting a lack of fit to the power law with $n = 2$ for open-cell solids, obtained by different random isotropic models. Deviation from the quadratic correlation was pointed out by several authors claiming the role of imperfections, irregularities or anisotropy in the cell arrangement (Grenestedt, 1998; Chen et al., 1999; Andrews et al., 1999).

Table 3 gives an outline of the results of the correlations obtained in the case of the studied parameters. Exponent values are significantly larger than the theoretical value for open cell solids. Although we can suppose that the cellular structures generated here are open over the range studied ($\rho < 0.35$), it is particularly noticed that n is sensitive to the value of ρ and that a fixed value of n is not possible in this range. This is inherent to structure generation which considers sphere packing instead of periodic arrangement of defined unit cells (Gibson and Ashby, 1997) and also probably to missing walls which decreases the value of Young's modulus for lower values of ρ (Silva and Gibson, 1997; Scanlon and Zghal, 2001). Nevertheless, a linear fitting procedure permitted to estimate n value as function of overlap distance and distribution width with an acceptable correlation factor ($r^2 = 0.88$):

$$n = 2.675 - 0.975 \times \delta - 2.240 \times \frac{\sigma}{r} \tag{8}$$

4.2. Comparison with experimental results obtained on food foams

In order to validate the approach of RSA in describing the structural features of open cell solids and relating them to elasticity modulus, the following application is tested. X-ray tomography structures of bread crumbs baked from different compositions are considered in order to obtain different cell structures (Fig. 10). The relative density varies in the range 0.17–0.31 (Table 4) and compression tests allowed to estimate the experimental values of Young's modulus, in the range 0.033–0.1 MPa (Fig. 11). Note that the relative density estimated experimentally using the procedure described in Babin et al. (2005) is less accurate than that directly calculated from tomography structures. Structures are meshed using the regular scheme described in Section 2.2 and the compression test is simulated under the same conditions as explained in Section 2.2. Young's modulus of the intrinsic material is calculated from the slope of stress–strain curve in the densification stage form compression tests of studied bread crumbs (Babin et al., 2005). A common average value of 0.64 MPa is obtained for all studied samples and is comparable to what is customary reported (Keetels et al., 1996; Scanlon and Zghal, 2001). Since no converging data are available from these references, an average value of the Poisson ratio is arbitrary fixed to 0.33.

An attempt to relate the Young's modulus predictions to structural effects is made by considering the equivalent RSA cellular solids. Firstly, the parameters σ/r, r_0 and average wall thickness are estimated from the 3D

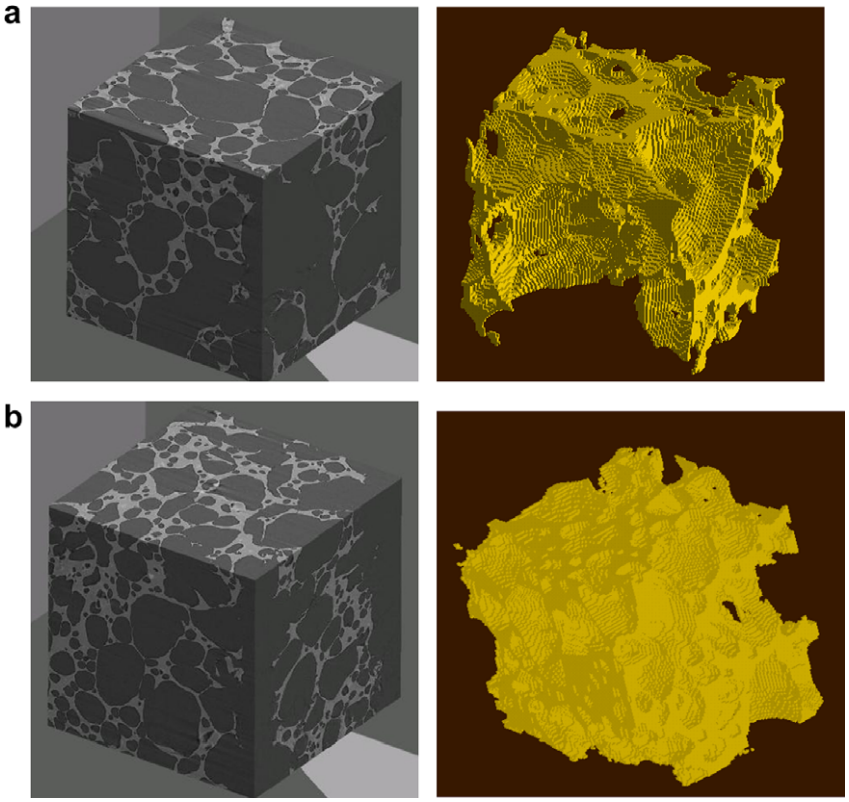

Fig. 10. Bread crumb porous structures determined using X-ray tomography and related meshed structures. (a) Sample #2 ($\rho = 0.17$). (b) Sample #3 ($\rho = 0.27$).

Table 4
Structure parameters and Young's modulus data of bread crumbs

Bread	Young's modulus		ρ		Wall thickness (μm)	σ (mm)	σ/r_0	δ (mm)	r_0 (mm)
	Pred.[a] (−)	Exp. (Pa)	Exp.	From 3D structures					
1	0.056	34925	0.20	0.18	241	1.5176	0.996	−0.21	1.523
2	0.029	33510	0.20	0.17	187	1.4173	1.123	−0.21	1.262
3	0.071	38865	0.21	0.27	219	1.4231	1.410	−0.14	1.010
4	0.022	34915	0.20	0.22	197	1.5000	1.577	−0.28	0.951
5	0.086	100705	0.31	0.31	209	1.5452	0.620	−0.07	0.84
6	0.055	47500	0.26	0.24	249	0.8866	0.900	−0.14	0.986

[a] The predicted relative Young's modulus is calculated with respect to an arbitrary solid phase Young's modulus.

images using the granulometry technique (Babin et al., 2005). Unfortunately, two-point correlation functions can not be derived using this technique and compared to PCF of simulated structures. The reason is inherent to the technique (Lassoued et al., 2007) and can be bypassed only if exact positions of overlapping voids are known. Labelling techniques fail in such computation whereas complex morphological operators as watershed (Russ and Russ, 1988; Serra, 1982) not addressed in this paper are of major interest. Secondly, a routine is used to calculate the lowest possible $|\delta|$ value corresponding to the set of experimental values for σ/r, ρ and r_0. In Table 4 are summarized the values of these parameters.

The comparison of the average predicted Young's modulus to the experimental one shows that despite a good agreement for two points ($\rho = 0.17$ and 0.24), a significant scatter is found. This scatter can be related to several factors. First, scaling effects might be inferred since computations were performed on cellular struc-

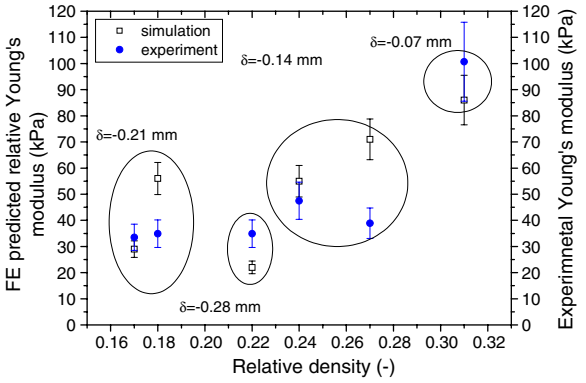

Fig. 11. Experimental and numerical Young's modulus of selected bread crumbs. Predicted minimum overlap distances are also shown. Relative density is estimated from 3D structures.

tures derived from 3D images having a volume of 0.15 cm^3, which might not be fully representative of the real crumb. The error on relative density might be linked to this preceding statement and it adds to the incertitude related to the experimental method of density measurement. Finally, the different crumbs were obtained from various formulations, the intrinsic Young's modulus of which may vary significantly although its experimental determination is difficult. Given these uncertainties, Fig. 11 reflects a fair agreement. It also indicates the predicted optimal δ values for each structure. The difference of $|\delta|$ values (0.28 and 0.14) explains the difference of stiffness obtained for close density values ($\rho = 0.22$–0.24 g cm^3, respectively), in agreement with the trend previously suggested (Fig. 9b).

5. Overall conclusions

The use of RSA to generate typical cellular solids suggests that cell organisation can vary significantly from random to organised architecture and cell wall size variability is expected. Anticipating the mechanical properties of cellular solids based on 3D image analysis requires not only an accurate estimation of mean size and dispersion of void size, but also indicators about void overlaps. This feature seems to control the overall Young's modulus of the open cell cellular solids having similar density. This variability explains the large deviation from the expected quadratic correlation between relative density and effective elasticity property.

Experimental evidence of the studied structural effects is not yet proved. The predicted results give only fair correlation with experimental ones in the case of bread crumbs, when taking the overlap distance into account. Apart from the effects discussed above, other effects such as cell wall waviness, plateau border variations can explain the observed scatter.

In a future work, a full structural characterization of real cellular products during deformation is planned in order to assess deformation mechanisms with respect to product design history.

References

Amon, M., Denson, C.D., 1984. A study of the dynamics of foam growth: analysis of the growth of closely spaced spherical bubbles. Polymer Engineering and Science 24, 1026–1034.

Andrews, E., Sanders, W.L., Gibson, J., 1999. Compressive and tensile behaviour of aluminum foams. Materials Science and Engineering A 270 (2), 113–124.

Babin, P., Della Valle, G., Dendievel, R., Lassoued, N., Salvo, L., 2005. Mechanical properties of bread crumbs from tomography based finite element simulations: mechanical behaviour of cellular solids. Journal of Materials Science 40, 5867–5873.

Brezny, R., Green, D.J., 1990a. The effect of cell size on the mechanical behavior of cellular materials. Acta Metallurgica et Materialia 38 (12), 2517.

Brezny, R., Green, D.J., 1990b. Characterization of edge effects in cellular materials. Journal of Materials Science 25, 4571–4578.

Chen, C., Lu, T.J., Fleck, N.A., 1999. Effect of imperfections on the yielding of two-dimensional foams. Journal of the Mechanics and Physics of Solids 47 (11), 2235–2272.

Clarke, A.S., Wiley, J.D., 1987. Numerical simulation of the dense random packing of a binary mixture of hard spheres: amorphous metals. Physical Review B 35, 7350–7356.

Dam, C.Q., Brezny, R., Green, D.J., 1990. Compressive behavior and deformation-mode map of an open cell alumina. Journal of Materials Research 5, 163–171.

Donev, A., Cisse, I., Sachs, D., Variano, E.A., Stillinger, F.H., Connelly, R., Torquato, S., Chaikin, P.M., 2004. Improving the Density of Jammed Disordered Packings Using Ellipsoids. Science 303, 990–993.

Evans, A.G., Hutchinson, J.W., Ashby, M.F., 1998. Cellular solids. Current Opinion in Solid State and Materials Science 3 (3), 288–303.

Evans, J.W., 1993. Random and cooperative sequential adsorption. Reviews of Modern Physics 65 (4), 1281–1329.

Gan, M., Gopinathan, N., Jia, X., Williams, R.A., 2004. Predicting Packing Characteristics of Particles of Arbitrary Shapes. KONA 22, 82–93.

Gibson, L.J., Ashby, M.F., 1997. Cellular solids. Pergamon Press Ltd, Cambridge.

Grenestedt, J.L., 1998. Influence of wavy imperfections in cell walls on elastic stiffness of cellular solids. Journal of the Mechanics and Physics of Solids 46 (1), 29–50.

Grenestedt, J.L., Bassinet, F., 2000. Influence of cell wall thickness variations on elastic stiffness of closed-cell cellular solids. International Journal of Mechanical Sciences 42 (7), 1327–1338.

Hagiwara, H., Green, D.J., 1987. Elastic Behavior of Open-Cell Alumina. Journal of American Ceramic Society 70, 811–815.

Jahne, B., 1997. Practical handbook on image processing for scientific applications. CRC Press, NY, pp. 589.

Kanit, T., Forest, S., Galliet, I., Mounoury, V., Jeulin, D., 2003. Determination of the size of the representative volume element for random composites: statistical and numerical approach. International Journal of Solids and Structures 40, 3647–3679.

Kanit, T., Guyen, F.N., Forest, S., Jeulin, D., Reed, M., Singleton, S., 2006. Apparent and effective physical properties of heterogeneous materials: Representativity of samples of two materials from food industryComput. Methods in Applied Mechanical Engineering 195, 3960–3982.

Keetels, C., vanVliet, T., Walstra, P., 1996. Relationship between the sponge structure of starch bread and its mechanical properties. Journal of Cereal Science 24, 27–31.

Lakes, R., 1995. In: Mühlhaus, H. (Ed.), Continuum models for materials with micro-structure. John Wiley, N.Y. Chapter 1, pp. 1–22.

Lassoued, N., Babin, P., Della Valle, G., Devaux, M.F., Reguerre, A.L., 2007. Granulometry of bread crumb grain: Contributions of 2D and 3D image analysis at different scale. Food Research International 40, 1087–1097.

Lavalle, P., Schaaf, P., Ostafin, M., Voegel, J.-C., Senger, B., 1999. Colloidal particles, sedimentation, fluctuation, radial distribution function. Proceedings of the National Academy of Sciences of the United States of America 96, 11100–11105.

Maire, E., Fazekas, A., Salvo, L., Dendievel, R., Youssef, S., Cloetens, P., Letang, J.M., 2003. X-ray tomography applied to the characterization of cellular materials. Related finite element modeling problems. Composites Science and Technology 63, 2431–2443.

Mattfeldt, T., Stoyan, D., 2000. Improved estimation of the pair correlation function of random sets. Journal of Microscopy 200, 158–173.

Monetto, I., Drugan, W.J., 2004. A micromechanics-based nonlocal constitutive equation for elastic composites containing randomly oriented spheroidal heterogeneities. Journal of the Mechanics and Physics of Solids 52, 359–393.

Onck, P.R., Andrews, E.W., Gibson, L.J., 2001. Size effects in ductile cellular solids. Part I: modelling. International Journal of Mechanical Sciences 43 (3), 681–699.

Poutet, J., Manzoni, D., Hage-Chehade, F., Thovert, J.-F., Adler, P.M., 1996. The effective mechanical properties of random porous media. Journal of the Mechanics and Physics of Solids 44 (10), 1587–1620.

Quintanilla, J., 2006. Measures of clustering in systems of overlapping particles. Mechanics of Materials 38, 849–858.

Roberts, A.P., Garboczi, E.J., 2001. Elastic moduli of model random three-dimensional closed-cell cellular solids. Acta Materialia 49 (2), 189–197.

Roberts, A.P., Garboczi, E.J., 2002. Elastic properties of model random three-dimensional open-cell solids. Journal of the Mechanics and Physics of Solids 50 (1), 33–55.

Russ, C., Russ, J., 1988. improved implementation of a convexx segmentation algorithm. Acta Stereologica 7, 33–40.

Russ, J.C., 1990. Computer-Assisted microscopy: The measurement and analysis of images. Plenum Press, NY, pp. 453.

Scanlon, M.G., Zghal, M.C., 2001. Bread properties and crumb structure. Food Research International 34 (10), 841–864.

Serra, J., 1982. image analysis and mathematical morphology. Academic press, London.

Sherwood, J.D., 1997. Packing of spheroids in three-dimensional space by random sequential addition. Journal of Physics A: Mathematical and General 30, L839–L843.

Silva, M., Gibson, L., 1997. the effect of non-periodic microstructure and defects on the compressive strength of two-dimensional cellular solids. International Journal of Mechanical Science 39, 549–563.

Stillinger, F.H., Torquato, S., 2004. Journal of Physical Chemistry B 108, 19589–19594.

Talbot, J., Schaaf, P., Tarjus, G., 1991. Random sequential addition of hard spheres. Molecular Physics 72 (6), 1397–1406.

Topping, B.H.V., Muylle, J., Putanowicz, R., Cheng, B., 2000. Finite Element Mesh Generation. Saxe-Coburg Publ., Edinburgh, pp. 250.

Williams, S.R., Philipse, A.P., 2003. Random packings of spheres and spherocylinders simulated by mechanical contraction. Physical Review E 67, 051301–051309.